COMPDYN 2013
4th ECCOMAS Thematic Conference on
Computational Methods in Structural Dynamics and Earthquake Engineering
M. Papadrakakis, V. Papadopoulos, V. Plevris (eds.)
Kos Island, Greece, 12–14 June 2013

FINITE ELEMENT MODELING OF LINEAR ELASTODYNAMICS PROBLEMS WITH EXPLICIT TIME-INTEGRATION METHODS AND LINEAR ELEMENTS WITH REDUCED DISPERSION. COMPARATIVE STUDY OF DIFFERENT FINITE ELEMENT TECHNIQUES USED FOR ELASTODYNAMICS.

Alexander V. Idesman

Texas Tech University
Box 41021, Lubbock, TX 79409, USA
e-mail: alexander.idesman@coe.ttu.edu

Keywords: elastic waves, numerical dispersion, explicit time integration, finite elements.

Abstract. *We have developed two finite element techniques with reduced dispersion for linear elastodynamics that are used with explicit time-integration methods. These techniques are based on the modified integration rule for the mass and stiffness matrices and on the averaged mass matrix approaches that lead to the numerical dispersion reduction for linear finite elements. The analytical study of numerical dispersion for the new techniques is carried out in the 1-D, 2-D and 3-D cases. The numerical study of the effectiveness of the dispersion reduction techniques includes two-stage time-integration approach with the filtering stage (developed in our previous papers) that quantifies and removes spurious high-frequency oscillations from numerical results. We have found that in contrast to the standard linear elements with explicit time-integration methods and the lumped mass matrix, the finite element techniques with reduced dispersion yield more accurate results at small time increments (smaller than the stability limit) in the 2D and 3-D cases. The advantages of the new technique are illustrated by the solution of the 1-D and 2-D impact problems. The new approaches with reduced dispersion can be easily implemented into existing finite element codes and lead to significant reduction in computation time at the same accuracy compared with the standard finite element formulations. Finally, we compare the accuracy of the linear elements with reduced dispersion, the spectral low- and high-order elements as well as the isogeometric elements by the solution of the 1-D impact problem. For all these solutions we use two-stage time integration technique with the filtering stage that removes spurious oscillations and allows an accurate comparison of different space discretization techniques used for elastodynamics. It is also interesting to mention that the amount of numerical dissipation at the filtering stage can be used as a quantitative measure for the comparison of accuracy of the different numerical formulations used for elastodynamics.*

1 INTRODUCTION

The application of the space discretization to transient acoustics or transient linear elastodynamics problems leads to a system of ordinary differential equations in time

$$\boldsymbol{M}\ddot{\boldsymbol{U}} + \boldsymbol{C}\dot{\boldsymbol{U}} + \boldsymbol{K}\boldsymbol{U} = \boldsymbol{R}, \tag{1}$$

where $\boldsymbol{M}$, $\boldsymbol{C}$, $\boldsymbol{K}$ are the mass, damping, and stiffness matrices, respectively, $\boldsymbol{U}$ is the vector of the nodal displacement, $\boldsymbol{R}$ is the vector of the nodal load. Zero viscosity, $\mathbf{C} = \mathbf{0}$, is considered in the paper. Due to the space discretization, the exact solution to Eq. (1) contains the numerical dispersion error; e.g., see [7, 9, 11, 26, 27, 28, 30, 31, 32, 14, 12] and others. The space discretization error can be decreased by the use of mesh refinement. However, this procedure significantly increases computational costs. Therefore, special techniques have been developed for the reduction in the numerical dispersion error which is also related to "the pollution effect" (e.g., see [1, 2, 10] and others for the study of the pollution error). One simple and effective technique for acoustic and elastic wave propagation problems is based on the calculation of the mass matrix $\boldsymbol{M}$ in Eq. (1) as a weighted average of the consistent and lumped mass matrices $\boldsymbol{M}$; see [26, 27, 28, 30] and others. For the 1-D case and linear finite elements, this approach reduces the error in the wave velocity for harmonic waves from the second order to the fourth order of accuracy. However, for harmonic wave propagation in the 2-D and 3-D cases, these results are not valid (nevertheless, in the multidimensional case, the averaged mass matrix yields more accurate results compared with the standard mass matrix; e.g., see the numerical results in Section 3). We should also mention that the known publications on the techniques with the averaged mass matrix do not include the effect of finite time increments on the dispersion error and on the accuracy of the numerical results. As shown in the current paper, if we use the weighting coefficients for the averaged mass matrix that are independent of time increments (as in the known approaches) and if the time increments for explicit time-integration methods are close to the stability limit then there is no advantages in the use of the averaged mass matrix compared with the lumped mass matrix.

An interesting technique with implicit and explicit time-integration methods is suggested in [32] for acoustic waves in the 2-D case. It is based on the modified integration rule for the calculation of the mass and stiffness matrices for linear finite elements. In contrast to the averaged mass matrix, the use of the modified integration rule increases the accuracy for the phase velocity from the second order to the fourth order in the general multi-dimensional case of acoustic waves. However, the applicability of this technique to elastodynamics problems has not been studied. The technique in [32] has not treated spurious oscillations that may significantly destroy the accuracy of numerical results.

We should mention that the analysis of numerical dispersion estimates the numerical error for propagation of harmonic waves. In the general case of loading (boundary conditions), the estimation of the accuracy of numerical techniques with reduced dispersion is difficult due to the presence of spurious high-frequency oscillations in numerical solutions; e.g., see [11, 26].

In our paper [17], we have described the finite element techniques with reduced dispersion for elastodynamics that are based on implicit time-integration methods with very small time increments. These techniques significantly reduce the computation time at the same accuracy compared with the standard finite element formulations with the consistent mass matrix. However, one of the disadvantages of the use of implicit time-integration methods is the necessity to solve a system of algebraic equations that can require large computational resources for a large number of degrees of freedom. In this paper we have extended the finite element techniques

with reduced dispersion that can be used with explicit time-integration methods. We have considered two techniques: one of them is based on the use of averaged mass matrix; another is based on the modified integration rule for the mass and stiffness matrices. In contrast to our paper [17], in the present paper we have also studied the effect of time increments on the accuracy of the numerical results.

2 THE FINITE ELEMENT TECHNIQUES WITH REDUCED DISPERSION FOR EXPLICIT TIME-INTEGRATION METHODS

Here we will present the averaged mass matrix technique and the modified integration rule technique that are used with explicit time-integration methods. These two techniques significantly reduce the numerical dispersion error and the computation time compared with the standard finite element formulations for linear elastodynamics. In contrast to the study of the averaged mass matrix technique and the modified integration rule technique for the scalar wave equation considered in [26, 32], the analytical study of these techniques for elastodynamics problems is much more complicated due to a greater number of non-linear terms in the dispersion equation for elastodynamics and the presence of two different types of waves (compressional and shear waves). For the use explicit time-integration methods (for simplicity we assume that the damping matrix is zero, $\boldsymbol{C} = \boldsymbol{0}$), we will first modify Eq. (1) similar to the paper [26]. Let's rewrite Eq. (1) with the diagonal (lumped) mass matrix $\boldsymbol{D}$ as follows

$$\boldsymbol{D}\dot{\boldsymbol{V}} + \boldsymbol{K}\boldsymbol{U} = \boldsymbol{R}, \tag{2}$$

where $\boldsymbol{V}$ is the vector of nodal velocity. Relationships between the nodal displacements and velocities can be written down as (similar to those in [26, 32])

$$\boldsymbol{D}\dot{\boldsymbol{U}} = \boldsymbol{M}\boldsymbol{V} \qquad \text{or} \qquad \boldsymbol{D}\ddot{\boldsymbol{U}} = \boldsymbol{M}\dot{\boldsymbol{V}} \tag{3}$$

where $\boldsymbol{M}$ is the non-diagonal mass matrix calculated by the averaged mass matrix technique (see Eq. (6) below) or by the modified integration rule technique (see Eqs. (7), (9) and (11) below). Inserting Eq. (3) into Eq. (2) we will get

$$\boldsymbol{D}\ddot{\boldsymbol{U}} + \boldsymbol{M}\boldsymbol{D}^{-1}\boldsymbol{K}\boldsymbol{U} = \boldsymbol{M}\boldsymbol{D}^{-1}\boldsymbol{R}. \tag{4}$$

Eq. (4) differs from the standard finite element equations with the lumped mass matrix by the stiffness matrix and the load vector which are multiplied by the term $\boldsymbol{M}\boldsymbol{D}^{-1}$. For the time integration of Eq. (4) we will use the standard explicit central-difference method (the most popular explicit method); e.g., see [20, 13, 3]. Replacing the second time derivative in Eq. (4) by the corresponding finite difference approximation used in the central-difference method, we obtain

$$\boldsymbol{D}\,[\boldsymbol{U}(t+\Delta t) - 2\boldsymbol{U}(t) + \boldsymbol{U}(t-\Delta t)]/\Delta t^2 + \boldsymbol{M}\boldsymbol{D}^{-1}\boldsymbol{K}\boldsymbol{U}(t) = \boldsymbol{M}\boldsymbol{D}^{-1}\boldsymbol{R}(t)\,, \tag{5}$$

where Δt is the time increment. Eq. (5) is used for the analysis of the numerical dispersion of the finite element formulations with the averaged mass matrix and modified integration rule techniques.

In order to decrease the numerical dispersion of finite element results, we consider the following two possibilities for the calculation of the mass and stiffness matrices: the mass matrix $\boldsymbol{M}$ is calculated as a weighted average of the consistent $\boldsymbol{M}^{cons}$ and lumped $\boldsymbol{D}$ mass matrices with the weighting factor γ (similar to that used in [26, 27, 30])

$$\boldsymbol{M}(\gamma) = \boldsymbol{D}\gamma + \boldsymbol{M}^{cons}(1-\gamma) \tag{6}$$

or the mass and stiffness matrices of each finite element are calculated with the modified integration rule (similar to those used in [32])

$$\boldsymbol{M}^e(\alpha_M) \,=\, \rho A \int\limits_{-1}^{1} \boldsymbol{N}^T(s)\boldsymbol{N}(s) det(\boldsymbol{J}) ds \,\approx \rho A \sum_{m=1}^{2} \boldsymbol{N}^T((-1)^m \alpha_M)\, \boldsymbol{N}((-1)^m \alpha_M) det(\boldsymbol{J})\,, \quad (7)$$

$$\boldsymbol{K}^e(\alpha_K) \,=\, \int\limits_{-1}^{1} E\boldsymbol{B}^T(s)\boldsymbol{B}(s) det(\boldsymbol{J}) ds \approx \sum_{m=1}^{2} E\boldsymbol{B}^T((-1)^m \alpha_K)\, \boldsymbol{B}((-1)^m \alpha_K) det(\boldsymbol{J}) \quad (8)$$

in the 1-D case,

$$\boldsymbol{M}^e(\alpha_M) \,=\, \rho b \int\limits_{-1}^{1}\int\limits_{-1}^{1} \boldsymbol{N}^T(s,t)\boldsymbol{N}(s,t) det(\boldsymbol{J}) ds dt$$

$$\approx \rho b \sum_{m=1}^{2}\sum_{j=1}^{2} \boldsymbol{N}^T((-1)^m \alpha_M, (-1)^j \alpha_M)\, \boldsymbol{N}((-1)^m \alpha_M, (-1)^j \alpha_M) det(\boldsymbol{J})\,, \quad (9)$$

$$\boldsymbol{K}^e(\alpha_K) \,=\, \int\limits_{-1}^{1}\int\limits_{-1}^{1} \boldsymbol{B}^T(s,t)\bar{\boldsymbol{C}}\boldsymbol{B}(s,t) det(\boldsymbol{J}) ds dt$$

$$\approx \sum_{m=1}^{2}\sum_{j=1}^{2} \boldsymbol{B}^T((-1)^m \alpha_K, (-1)^j \alpha_K)\, \bar{\boldsymbol{C}}\boldsymbol{B}((-1)^m \alpha_K, (-1)^j \alpha_K) det(\boldsymbol{J}) \quad (10)$$

in the 2-D case,

$$\boldsymbol{M}^e(\alpha_M) \,=\, \rho \int\limits_{-1}^{1}\int\limits_{-1}^{1}\int\limits_{-1}^{1} \boldsymbol{N}^T(s,t,q)\boldsymbol{N}(s,t,q) det(\boldsymbol{J}) ds dt dq$$

$$\approx \rho \sum_{m=1}^{2}\sum_{j=1}^{2}\sum_{p=1}^{2} \boldsymbol{N}^T((-1)^m \alpha_M, (-1)^j \alpha_M, (-1)^p \alpha_M)\, \boldsymbol{N}((-1)^m \alpha_M, (-1)^j \alpha_M, (-1)^p \alpha_M) det(\boldsymbol{J})\,, \quad (11)$$

$$\boldsymbol{K}^e(\alpha_K) \,=\, \int\limits_{-1}^{1}\int\limits_{-1}^{1}\int\limits_{-1}^{1} \boldsymbol{B}^T(s,t,q)\bar{\boldsymbol{C}}\boldsymbol{B}(s,t,q) det(\boldsymbol{J}) ds dt dq$$

$$\approx \sum_{m=1}^{2}\sum_{j=1}^{2}\sum_{p=1}^{2} \boldsymbol{B}^T((-1)^m \alpha_K, (-1)^j \alpha_K, (-1)^p \alpha_K)\, \bar{\boldsymbol{C}}\boldsymbol{B}((-1)^m \alpha_K, (-1)^j \alpha_K, (-1)^p \alpha_K) det(\boldsymbol{J}) \quad (12)$$

in the 3-D case. Here, $\boldsymbol{N}$ and $\boldsymbol{B}$ are the standard finite element shape and B matrices; $\bar{\boldsymbol{C}}$ is the matrix of elastic coefficients:

$$\bar{\boldsymbol{C}} \,=\, \frac{E(1-\nu)}{(1+\nu)(1-2\nu)} \begin{pmatrix} 1 & \frac{\nu}{1-\nu} & 0 \\ \frac{\nu}{1-\nu} & 1 & 0 \\ 0 & 0 & \frac{1-2\nu}{2(1-\nu)} \end{pmatrix}$$

in the 2-D case of plane strain and

$$\bar{\boldsymbol{C}} \,=\, \frac{E(1-\nu)}{(1+\nu)(1-2\nu)} \begin{pmatrix} 1 & \frac{\nu}{1-\nu} & \frac{\nu}{1-\nu} & 0 & 0 & 0 \\ \frac{\nu}{1-\nu} & 1 & \frac{\nu}{1-\nu} & 0 & 0 & 0 \\ \frac{\nu}{1-\nu} & \frac{\nu}{1-\nu} & 1 & 0 & 0 & 0 \\ 0 & 0 & 0 & \frac{1-2\nu}{2(1-\nu)} & 0 & 0 \\ 0 & 0 & 0 & 0 & \frac{1-2\nu}{2(1-\nu)} & 0 \\ 0 & 0 & 0 & 0 & 0 & \frac{1-2\nu}{2(1-\nu)} \end{pmatrix}$$

in the 3-D case; the diagonal terms of the lumped mass matrix $\boldsymbol{D}$ (except those for the boundary nodes) for the linear elements are dx; dx^2; dx^3 in the 1-D case, in the 2-D case for square elements and in the 3-D case for cubic elements, respectively; $\boldsymbol{J}$ is the Jacobian matrix ($det(\boldsymbol{J}) = dx/2$; $dx^2/4$; $dx^3/8$ in the 1-D case, in the 2-D case for square elements and in the 3-D case for cubic elements, respectively; dx is the length of a finite element); A is the cross sectional area in the 1-D case; b is the thickness in the 2-D case of plane strain; s, t, q are the isoparametric coordinates; α_M and α_K are the coordinates of the integration points for the mass and stiffness matrices to be determined (2, $2 \times 2 = 4$ and $2 \times 2 \times 2 = 8$ integration points are used for linear elements in the 1-D, 2-D and 3-D cases, respectively); e.g., see [13, 3] for the derivation of finite element matrices. The integration error due to the application of the modified integration rule for the mass and stiffness matrices does not change the convergence rate of finite element solutions; see [32].

We use the dispersion analysis in order to find such γ, α_M and α_K that reduce the numerical dispersion error. The results of the dispersion analysis considered in detail in our paper [21] are summarized below. In the 1-D case, the numerical dispersion error decreases at $\gamma = \gamma^{opt} = \frac{3-\bar{\tau}^2}{2}$ and at $\alpha_M = \alpha_M^{opt} = \sqrt{\frac{4-\bar{\tau}^2}{3}}$ where $\bar{\tau} = \frac{c_o \Delta t}{dx}$ is the Courant number, dx is the size of a finite element, Δt is the size of a time increment, c_o is $c_o = \sqrt{E/\rho}$ is the wave velocity in the 1-D case, ρ is the density, E is Young's modulus. We should mention that at $\bar{\tau} \approx 0$ (for very small time increments), the optimal value of $\gamma^{opt} = \frac{3}{2}$ coincides with the results obtained in [26] for the 1-D case. However, the size of time increments may significantly affect γ^{opt}. For example, the stability limit for the time integration of Eq. (5) on uniform meshes with linear elements equals $\Delta t^{st} = \frac{dx}{c_o}$ or $\bar{\tau} = 1$. In this case, $\gamma^{opt} = 1$ and $\boldsymbol{M} = \boldsymbol{D}$ (see Eq. (6)); i.e., for this particular case, Eq. (5) reduces to the standard finite element formulation with the lumped mass matrix (it is known that in the 1-D case, the standard linear finite elements and the explicit central difference method yields the exact solution to the 1-D impact problem at $\bar{\tau} = 1$; e.g., see [13]). It can be also shown that for linear elements with the averaged mass matrix and 1-D uniform meshes, the dispersion error increases with the decrease in the size of time increments Δt for time increments smaller than the stability limit. At $\gamma = (3\alpha_M^2 - 1)/2$ (with the optimal value of $\alpha_M^{opt} = \sqrt{\frac{4-\bar{\tau}^2}{3}}$ or the same as in [32]), the modified integration rule and the average mass matrix techniques yield the same results and are completely equivalent in the 1-D case.

In the multi-dimensional case, the numerical dispersion error decreases at $\alpha_M = \sqrt{\frac{4-\tau^2}{3}}$ and $\alpha_K = \sqrt{\frac{4(2\nu-1)}{3(4\nu-3)}}$ for the modified integration rule and $\gamma = \frac{3-\tau^2}{2}$ for the averaged mass matrix technique where $\tau = \frac{c_2 \Delta t}{dx}$, $c_2 = \sqrt{\frac{E}{2\rho(1+\nu)}}$ is the phase velocity of the shear waves and ν is Poisson's ratio. In contrast to the 1-D case, the dispersion error decreases with the decrease in time increments; see [21].

3 NUMERICAL MODELING

The new finite element techniques with reduced dispersion are implemented into the finite element code FEAP [33]. Below they are applied to 1-D and 2-D impact linear elastodynamics problems for which all low and high frequencies are excited. Due to spurious high-frequency oscillations, these problems cannot be accurately solved by existing time-integration methods based on the introduction of artificial viscosity (or numerical dissipation) at each time increment, especially in the case of long-term integration. Therefore, the two-stage time integration technique developed in our previous papers [22, 18, 20] (see also the Appendix) is used. The filtering stage of this technique includes the time-continuous Galerkin (TCG) method with

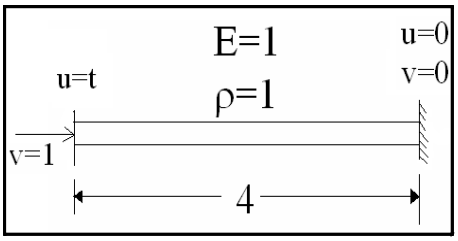

Figure 1: Impact of an elastic bar of length $L = 4$ against a rigid wall.

$N = 10$ time increments (5 positive plus 5 negative time increments) the size of which is calculated according to Eqs. (13) - (15) (see [22, 18, 20] and the Appendix below). We also compare the numerical results obtained by the linear elements with reduced dispersion (see Section 2), by the spectral low- and high-order elements (e.g., see [6, 23, 24, 25, 29] and others) and by the isogeometric elements (e.g., see [4, 5, 8, 14] and others).

3.1 1-D impact of an elastic bar against a rigid wall

The impact of an elastic bar of the length $L = 4$ and the cross section $A = 1$ against a rigid wall is considered in the 1-D case (see Fig. 1). Young's modulus is chosen to be $E = 1$ and the density to be $\rho = 1$. The following boundary conditions are applied: the displacement $u(0, t) = t$ (which corresponds to the velocity $v(0, t) = v_0 = 1$) and $u(4, t) = 0$ (which corresponds to the velocity $v(4, t) = 0$). Initial displacements and velocities are zero; i.e., $u(x, 0) = v(x, 0) = 0$. The analytical solution to this problem for time $0 \le t \le L\sqrt{\rho/E} = 4$ includes the continuous variation of displacements $u_a(x, t) = t - x$ for $t \ge x$ and $u_a(x, t) = 0$ for $t \le x$, and the piecewise constant variation of velocities and stresses $v_a(x, t) = -\sigma^a(x, t) = 1$ for $t \ge x$ and $v_a(x, t) = \sigma^a(x, t) = 0$ for $t \le x$ (at the interface $x = t$, jumps in stresses and velocities occur). For time $4 \le t \le 8$ the solution is similar to that for $0 \le t \le 4$ with the difference that the elastic wave reflects from the right end and propagates to the left. For time $8 \le t \le 12$ the solution is the same as for time $0 \le t \le 4$ and so on. In order to compare the results at short- and long-term integrations, the observation times are chosen to be $T = 2; 18; 98; 194$. The exact distributions of the velocities and stresses along the bar are the same at these observation times and correspond to the location of the wave front in the middle of the bar.

Along with the linear elements with reduced dispersion described in Section 2, we will solve the 1-D impact problem using the spectral low- and high-order elements (up to the 10th-order). For these space-discretization methods, the diagonal mass matrices and the explicit central-difference method with very small time increments are used. We should also mention that the spectral 1st- and 2nd-order elements coincide with the standard finite elements of the same orders. For the comparison of accuracy, we will also present the results obtained by the isogeometric 3rd-order elements with the consistent (non-diagonal) mass matrix and the implicit time-integration method with very small time increments. Uniform meshes with 101 degrees of freedom (dof) are used for all types of elements; see Figs. 2 - 6. In addition to these meshes, we also use uniform meshes with 201, 301 and 401 dof for the linear elements with reduced dispersion; see Fig. 5. Figs. 2 - 4 show the numerical solutions for the velocity at different observation times. All space-discretization methods yield spurious oscillations after basic computations and the amplitudes of these oscillations increase with the increase in the observation time; see Figs. 2a,b - 4a,b. The slope of the wave front in the basic computations is steeper for short observation times and is more diffusive for large observation times. The filtering stage

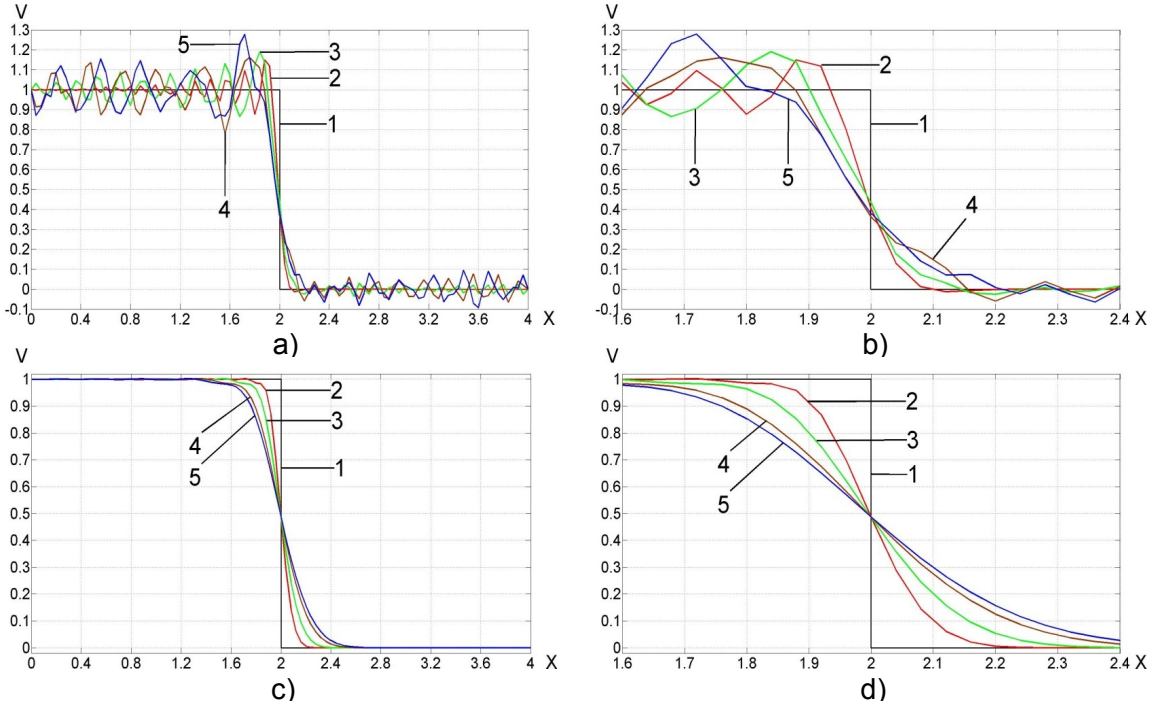

Figure 2: The velocity distribution along the bar after (a, b) basic computations (the lumped mass matrix and small time increments) and after (c, d) post-processing. A uniform mesh with the linear elements with reduced dispersion and 101 dof is used. Curves 1 correspond to the analytical solutions. Curves 2, 3, 4 and 5 correspond to the observation times $T = 2,\ 18,\ 98$ and 194, respectively. b) and d) show the zoomed graphs a) and c) in the range $1.6 < x < 2.4$.

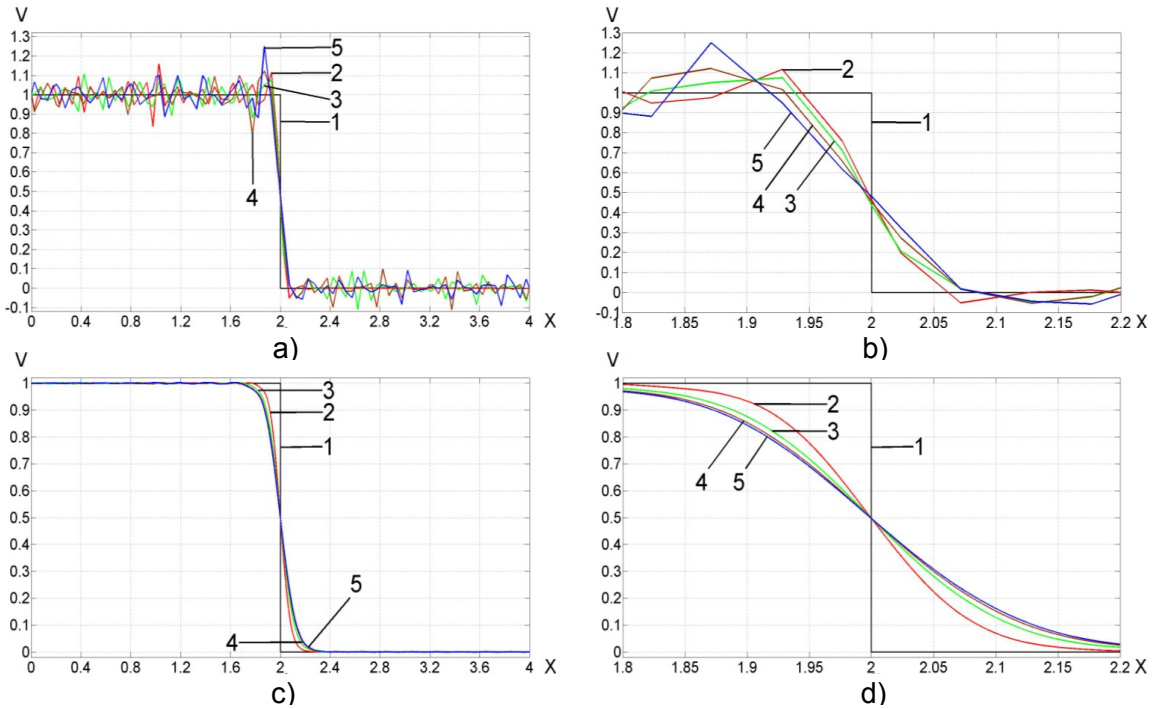

Figure 3: The velocity distribution along the bar after (a, b) basic computations (the lumped mass matrix and small time increments) and after (c, d) post-processing. A uniform mesh with the spectral 5th-order elements and 101 dof is used. Curves 1 correspond to the analytical solutions. Curves 2, 3, 4 and 5 correspond to the observation times $T = 2,\ 18,\ 98$ and 194, respectively. b) and d) show the zoomed graphs a) and c) in the range $1.8 < x < 2.2$.

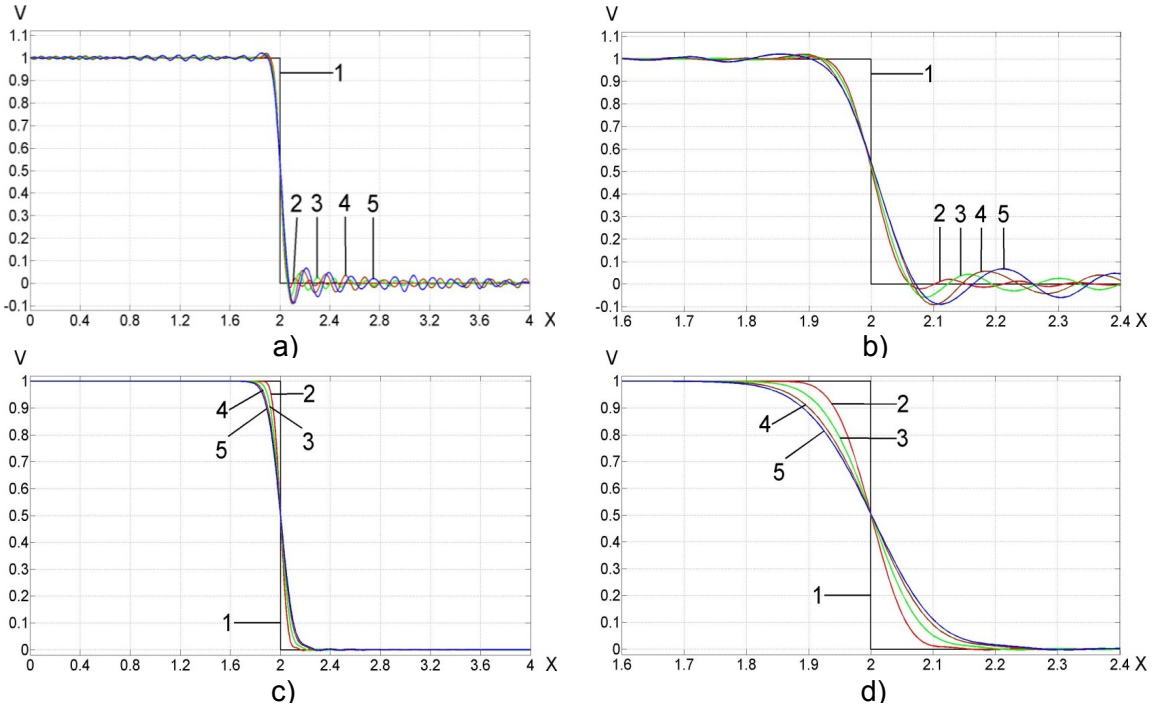

Figure 4: The velocity distribution along the bar after (a, b) basic computations (the consistent mass matrix and small time increments) and after (c, d) post-processing. A uniform mesh with the isogeometric 3rd-order elements and 101 dof is used. Curves 1 correspond to the analytical solutions. Curves 2, 3, 4 and 5 correspond to the observation times $T = 2,\ 18,\ 98$ and 194, respectively. b) and d) show the zoomed graphs a) and c) in the range $1.6 < x < 2.4$.

removes the spurious oscillations. However, despite the same analytical solutions at the selected observation times, the numerical results after the filtering stage are more accurate for short observation times than those for large observation times; see Figs. 2c,d - 4c,d. Because the error in time is very small in these calculations and can be neglected, the difference in the numerical results for different observation times is due to the space-discretization error (which is also related to the dispersion error). This difference is also smaller for higher-order elements compared with lower-order elements (the dispersion error for higher-order elements is smaller).

Fig. 5a,b shows that at the same number 101 of dof, the increase in the order of the spectral elements improves the accuracy; see curves 3-7. At the same number of dof, the linear elements with reduced dispersion are slightly more accurate than the standard 2nd-order elements with the lumped mass matrix; see curves 2 and 4 in Fig. 5a,b. Fig. 5c,d also shows that the linear elements with reduced dispersion and 201 dof are more accurate than the spectral 5th-order elements with 101 dof at time $T = 18$ and are slightly less accurate than the spectral 5th-order elements with 101 dof at the large observation time $T = 194$; see curves 2 and 6. Similarly, the linear elements with reduced dispersion and 301 dof are more accurate than the spectral 10th-order elements with 101 dof at time $T = 18$ and yield practically the same accuracy as the spectral 10th-order elements with 101 dof at the large observation time $T = 194$; see curves 3 and 7.

For the explicit time integration, the computations are very often implemented on the level of elements without the calculation of the global mass and stiffness matrices. Therefore, the computation cost in this case is related to the multiplication of the local effective stiffness matrix by a non-zero vector and is proportional to $n_{dof}^2 n_{el}$ where n_{dof} is the the number of dof for one element and n_{el} is the number of elements. For example, $n_{dof}^2 n_{el} = 11^2 \cdot 10 = 1210$ for the

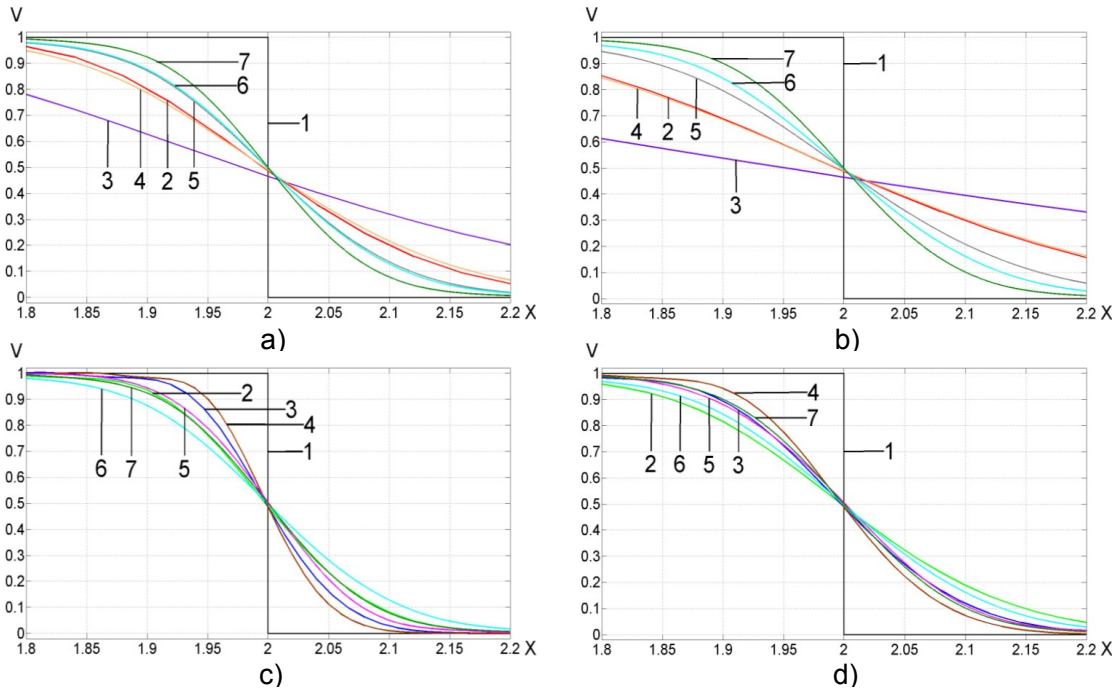

Figure 5: The velocity distribution along the bar in the range $1.8 < x < 2.2$ at the observation times $T = 18$ (a, c) and $T = 194$ (b, d) after post-processing. Curves 1 correspond to the analytical solutions. Curves 2 in (a, b), 2 in (c, d), 3 in (c, d) and 4 in (c, d) correspond to the linear elements with reduced dispersion (the lumped mass matrix) with 101, 201, 301 and 401 dof, respectively. Curves 3 in (a, b), 4 in (a, b), 5 in (a, b), 6 and 7 correspond to the spectral linear, quadratic, 4th-order, 5th-order and 10th-order elements with 101 dof. Curves 5 in (c, d) correspond to the isogeometric 3rd-order elements with 101 dof.

spectral 10th-order elements with 101 dof and $n_{dof}^2 n_{el} = 2^2 \cdot 300 = 1200$ for the linear elements with reduced dispersion and 301 dof; i.e., the computational costs are approximately the same in this case. However, we can also reduce the computational cost for the linear elements with reduced dispersion by the use of the following procedure. Let us combine every 30 linear elements (e.g., staring from the left end of the bar) into one superelement. In this case we will obtain $n_{el} = 10$ superelements. The computation cost for $n_{el} = 10$ superelements is $n_{dof} b n_{el} = 31 \cdot 2 \cdot 10 = 620$ where $n_{dof} = 31$ is the number of dof of one superelement and $b = 2$ is the bandwidth of the effective stiffness matrix of one superelement consisting of 30 linear elements with reduced dispersion. This means that at the same or better accuracy (e.g, see curves 3 and 7 in Fig. 5c,d at the observation times $T = 18$ and $T = 194$), the linear elements with reduced dispersion and 301 dof require less computation time and are more computationally effective compared with the spectral 10th-order elements with 101 dof at times $T = 18$ and $T = 194$.

In order to compare the accuracy of the numerical results obtained with the different space-discretization techniques as well as with the diagonal and non-diagonal mass matrices, Fig. 5c,d also includes the numerical solutions obtained by the isogeometric 3rd-order elements (the non-diagonal mass matrix) with 101 dof. As can be seen, the accuracy of the isogeometric 3rd-order elements at time $T = 18$ and $T = 194$ is close to that of the spectral 10th-order elements at the same number of dof; see curves 5 and 7.

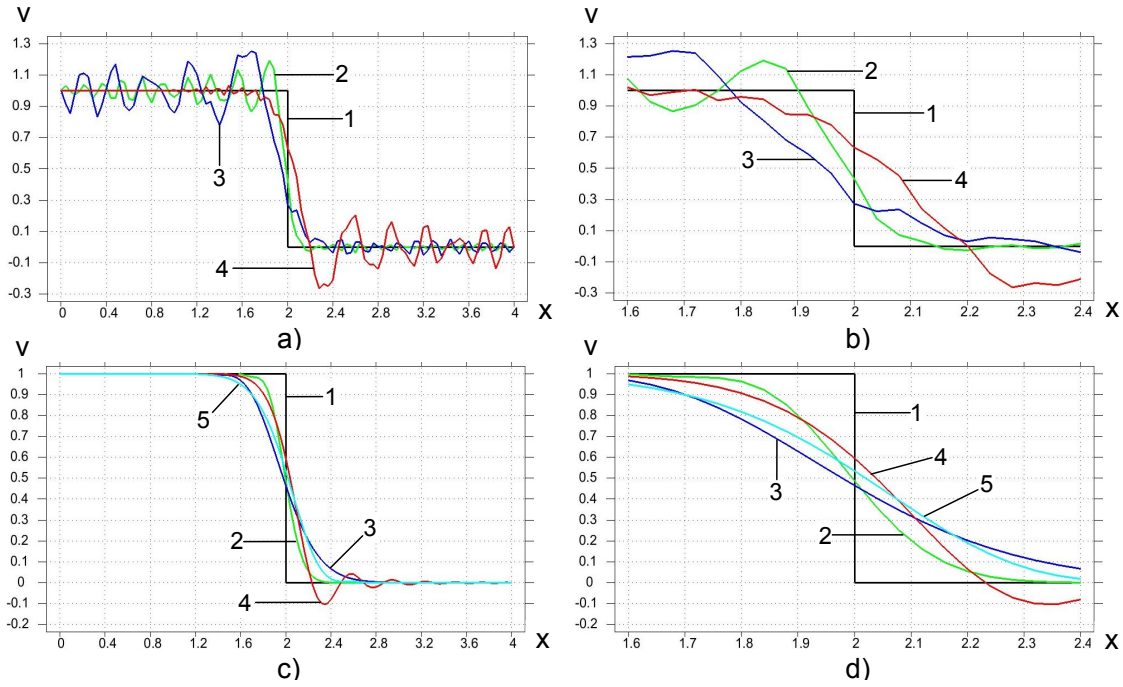

Figure 6: The velocity distribution along the bar at observation time $T = 18$ after basic computations (a, b) and after post-processing (c, d). A uniform mesh with 100 linear 2-node finite elements is used. Curves 1 correspond to the analytical solution. Curves 2 and 3 correspond to the numerical solutions with the averaged ($\gamma = \frac{3-\tau^2}{2}$) and lumped mass matrices (with small time increments $\Delta t = \Delta t^{st}/20$ in basic computations). Curves 4 correspond to the numerical solutions for the averaged ($\gamma = 1.5$) mass matrix and the time increments in basic computations close to the stability limit. b) and d) show the zoomed graphs a) and c) in the range $1.6 < x < 2.4$. Curves 4 and 5 in c) and d) differ by the amount of numerical dissipation used at the filtering stage; see the text.

It is interesting to note that the size of time increments at the filtering stage calculated according to the formulas Eqs. (13) - (14) from the Appendix indirectly defines the range of actual frequencies used in numerical solutions and can be used for the comparison of the accuracy of different space-discretization techniques; see our papers [17, 20, 21]. If at the selected observation time T the time increment at the filtering stage for one space-discretization technique is smaller than that for another space-discretization technique then the former technique yields more accurate results at time T than the latter technique (if time increments are close to each other then the techniques yield approximately the same results). This means that Eqs. (13) - (14) allow the quantitative comparison of the accuracy of different space-discretization techniques. For example, according to Eqs. (13) - (14), we use the following time increments for the filtering stage at time $T = 18$: $\Delta t_1 = 0.0405$, $\Delta t_2 = 0.0235$, $\Delta t_3 = 0.0171$ and $\Delta t_4 = 0.0137$ for the linear elements with reduced dispersion (the diagonal mass matrix) with 101 dof, 201 dof, 301 dof and 410 dof, respectively; $\Delta t_5 = 0.0448$ for the standard quadratic elements (the diagonal mass matrix) with 101 dof; $\Delta t_6 = 0.0222$ for the spectral 10th-order elements (the diagonal mass matrix) with 101 dof; $\Delta t_7 = 0.0188$ for the isogeometric 3rd-order elements (the consistent mass matrix) with 101 dof. At the large observation time $T = 194$, we have the following time increments for the filtering stage: $\Delta t_1 = 0.0679$, $\Delta t_2 = 0.0395$, $\Delta t_3 = 0.0288$ and $\Delta t_4 = 0.0230$ for the linear elements with reduced dispersion (the diagonal mass matrix) with 101 dof, 201 dof, 301 dof and 410 dof, respectively; $\Delta t_5 = 0.0695$ for the standard quadratic elements (the diagonal mass matrix) with 101 dof; $\Delta t_6 = 0.0266$ for the spectral 10th-order elements (the diagonal mass matrix) with 101 dof; $\Delta t_7 = 0.0269$ for the isogeometric 3rd-order

elements (the consistent mass matrix) with 101 dof. Comparing these time increments at the same observation time, we can describe the accuracy of the numerical results discussed above. For example, at times $T = 18$ and $T = 194$, the time increments Δt_6 and Δt_7 are close to each other and the corresponding space-discretization techniques yield approximately the same accuracy; see curves 5 and 7 in Fig. 5c,d (similar results we have for the time increments Δt_1 and Δt_5; see curves 2 and 4 in Fig. 5a,b). We also have that $\Delta t_3 < \Delta t_6$ at time $T = 18$ and $\Delta t_3 > \Delta t_6$ at time $T = 18$ (see curves 3 and 7 in Fig. 5c,d and the comparison of the spectral elements and the elements with reduced dispersion described above in this section). It can be also seen that Δt_4 has the smallest value among all presented time increments and the corresponding linear elements with reduced dispersion and 401 dof yield the most accurate results; see curves 4 in Fig. 5c,d.

In Fig. 6, we have also analyzed the numerical results for the averaged mass matrix with $\gamma = \frac{3}{2}$ (as suggested in [26]) and the explicit central difference method with time increments close to the stability limit Δt^{st} at basic computations. As we can see, in this case the results after basic computations (curve 4 in Fig. 6a,b) are less accurate than those described by curve 2 in Fig. 6a,b. If we filter these results (curve 4 in Fig. 6a,b) with the amount of numerical dissipation (time increments) used for curve 2 in Fig. 6a,b, then spurious oscillations remain after the filtering stage (curve 4 in Fig. 6c,d). If we use a sufficient amount of numerical dissipation at the filtering stage then the results (curve 5 in Fig. 6c,d) are close to curve 3 in Fig. 6c,d. This means that the approach suggested in [26]) for the averaged mass matrix does not improve the dispersion error and the accuracy of numerical results if relative large time increments (close to the stability limit) are used in calculations. However, at small time increments $\Delta t \approx 0$, parameter $\tau \approx 0$ is also small and $\gamma = \frac{3-\tau^2}{2} \approx \frac{3}{2}$; i.e., the results for $\gamma = \frac{3}{2}$ will coincide with curve 2 in Fig. 6 at small time increments in basic computations.

3.2 2-D impact of an elastic bar against a rigid wall (plane strain)

This problem is a more general plane strain formulation of the 1-D impact problem considered in Section 3.1; see Fig. 7a. In contrast to the 1-D impact problem, compressional and shear elastic waves propagate in the 2-D case.

A bar of length $L = 4$ and height $2H = 2$ is considered. Due to symmetry, the problem is solved for a half of the bar $ABCD$ where AD is the axis of symmetry. Young's modulus is chosen to be $E = 1$, the density to be $\rho = 1$ and Poisson's ratio to be $\nu = 0.3$. The following boundary conditions are applied: along boundary AB $u_n = t$ (it corresponds to velocity $v_n = v_0 = 1$) and $\tau_n = 0$; along boundaries BC and CD $\sigma_n = 0$ and $\tau_n = 0$; along boundary AD $u_n = 0$ and $\tau_n = 0$, where u_n, v_n, and σ_n are the normal displacements, velocities and the tractive forces, respectively; τ_n are the tangential tractive forces. Initial displacements and velocities are zero; i.e., $u(x, y, 0) = v(x, y, 0) = 0$. The observation time is chosen to be $T = 13$. During this time the velocity pulse travels within the bar with multiple reflections from the ends of the bar and from the external surface BC.

The problem is solved on uniform meshes with $40 \times 160 = 6400$ and $120 \times 480 = 57600$ linear four-node quadrilateral finite elements with the modified integration rule for the mass and stiffness matrices ($\alpha_M = \sqrt{\frac{4-\tau^2}{3}}$ and $\alpha_K = \sqrt{\frac{4(2\nu-1)}{3(4\nu-3)}}$) and with the lumped and averaged ($\gamma = \frac{3-\tau^2}{2}$) mass matrices. In order to study the effect of time increments at basic calculations on the accuracy of numerical results, we will use time increments $\Delta t \approx \Delta t^{st}$ close to the stability limit Δt^{st} and very small time increments $\Delta t = \Delta t^{st}/20$).

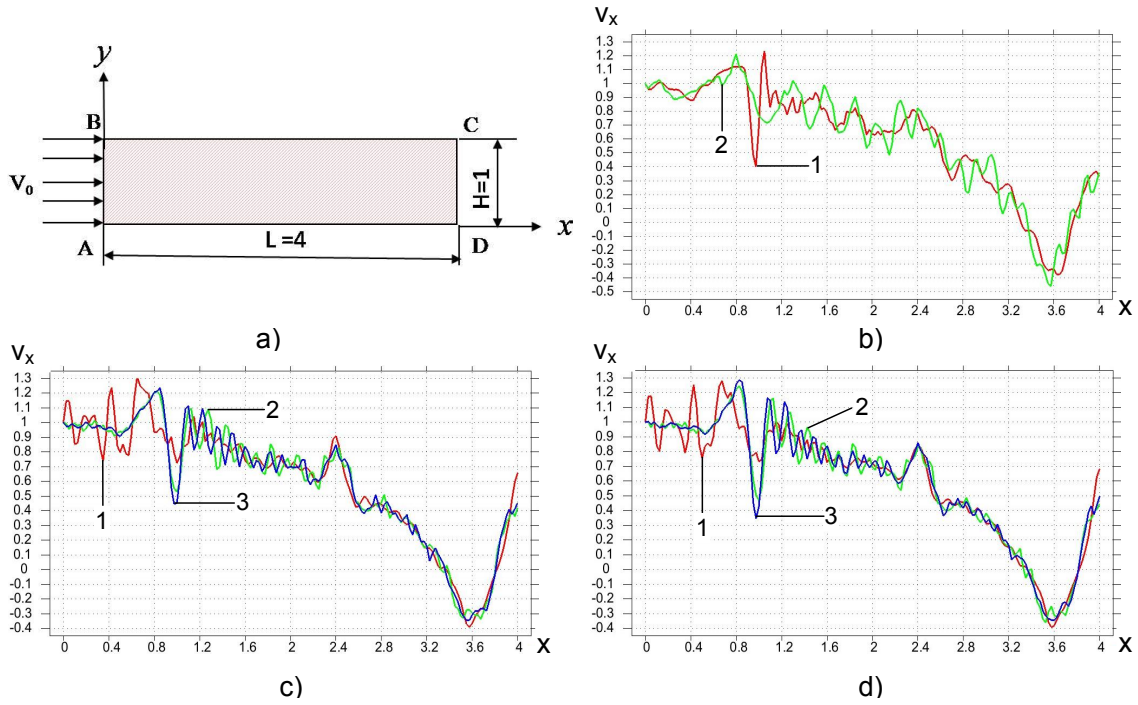

Figure 7: A 2-D plane strain impact problem (a). The axial velocity distribution along the axis of symmetry AD at observation time $T = 13$. The results are shown after basic computations obtained by the explicit central difference method with the lumped mass matrix (b), with the modified integration rule (c), and with the averaged mass matrix (d). Curves 1 and 2 correspond to the numerical solutions obtained with the time increments Δt^{st} and $\Delta t^{st}/20$, respectively. Curves 3 correspond to the numerical solutions (from our paper [20]) obtained by the implicit time-integration method with the modified integration rule (c) and the averaged mass matrix (d). A uniform mesh with $40 \times 160 = 6400$ linear 4-node finite elements is used.

Figs. 7 - 8 show the distribution of the axial velocity along the axis of symmetry AD at observation time $T = 13$ after basic computations (Fig. 7) and after the filtering stage (Fig. 8). Similar to the previous 1-D impact problem, the numerical results after basic computations with the lumped stiffness matrix and the formulations with reduced numerical dispersion contain spurious oscillations at very small time increments $\Delta t = \Delta t^{st}/20 = \frac{dx}{20c_1}$; see curves 2 in Fig. 7. However, in contrast to the 1-D impact problem, the spurious oscillations and the dispersion error at basic computations do not disappear at the time increments close to the stability limit; see curves 1 in Fig. 7. It also can be seen from Fig. 7 (see curves 1 and 2) that the results after basic computation for the time increments close to the stability limit and for very small time increments are different for all methods. We should also note that at very small time increments, the numerical solutions for the linear elements with reduced dispersion obtained with the explicit central difference method (curves 2 in Fig. 7c,d) and with the implicit trapezoidal rule (see our paper [17] as well as curves 3 in Fig. 7c,d) are close to each other. However, it is difficult to compare the accuracy of different approaches after basic computations due to large spurious oscillations.

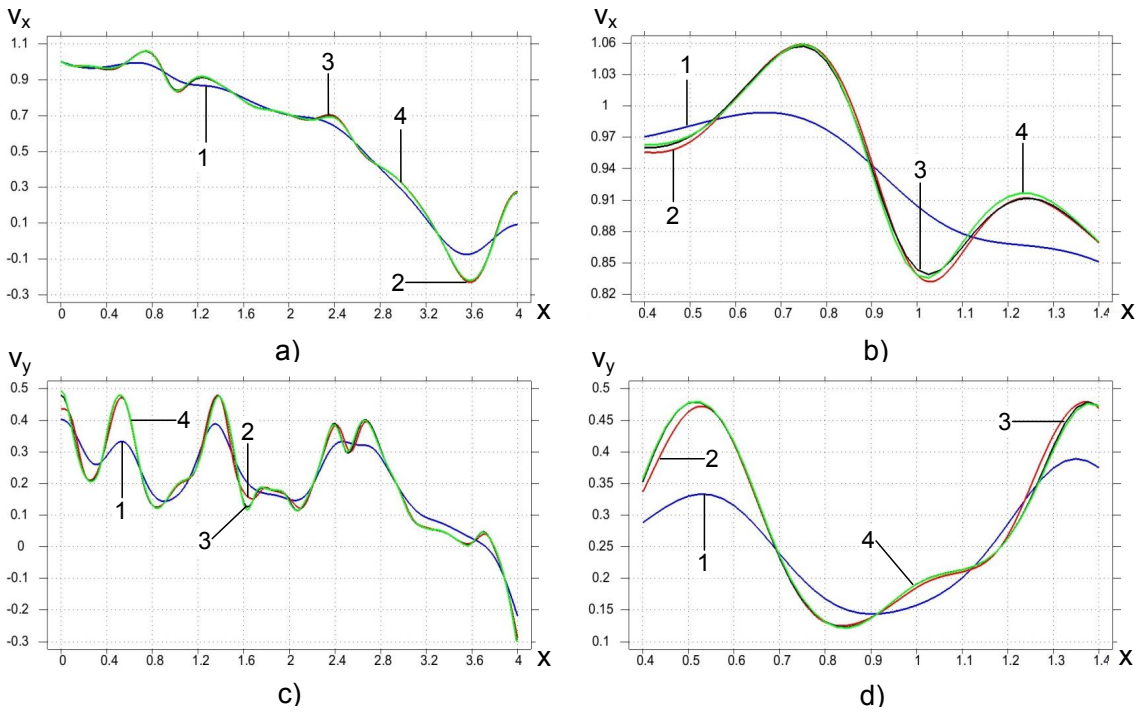

Figure 8: The axial velocity distribution v_x along the axis of symmetry AD (a, b) and the transverse velocity distribution v_y along the external surface BC (c, d) at observation time $T = 13$ for the Poisson's ratio $\nu = 0.3$. The results are shown after the filtering of the solutions at basic computations obtained by the explicit central difference method with the lumped mass matrix (curves 1 and 2), with the modified integration rule (curve 3), and with the averaged mass matrix (curve 4). Small time increments $\Delta t^{st}/20$ are used at basic computations (see Fig. 7). Uniform meshes with $40 \times 160 = 6400$ (curves 1, 3 and 4) and $120 \times 480 = 57600$ (curve 2) linear elements are used. b) and d) show the zoomed graphs a) and c) in the range $0.4 < x < 1.4$.

After filtering spurious oscillations at the filtering stage, the solutions at basic computations obtained by the explicit central difference method at very small time increments $\Delta t^{st}/20$ with the modified integration rule (curves 3 in Fig. 8) and with the averaged mass matrix (curves 4 in Fig. 8) are close to each other. The results in Fig. 8 show that despite the impact along the x-axis elastic waves propagate in all directions and the magnitudes of the transverse velocity v_y are comparable with those for the axial velocity v_x; i.e., a general case of propagation of elastic waves occurs for the considered problem. As can be seen from Fig. 8, after the filtering stage the results obtained by the explicit central difference method at very small time increments $\Delta t^{st}/20$ and the lumped mass matrix (curves 1) are much less accurate than those obtained with the elements with reduced dispersion (curves 3 and 4). The results obtained by the standard approach with the explicit central difference method on a fine mesh with $120 \times 480 = 57600$ linear elements (curves 2 in Fig. 8) show that at the selected observation time, the elements with reduced dispersion reduce the number of degrees of freedom by a factor of 9 compared with those for the standard approach at the same accuracy (compare curves 3 or 4 for a mesh with $40 \times 160 = 6400$ linear elements and curves 2 for a mesh with $120 \times 480 = 57600$ linear elements in Fig. 8).

Remark. Similar to the 1-D case in Section 3.1 and the results reported in our paper [17] for implicit time-integration methods, the size of the time increments calculated by Eqs. (13) - (15) for the filtering stage allows the quantitative estimation of the advantage of the modified integration rule (or the averaged mass matrix) technique compared with the standard lumped mass matrix. For example, for a uniform mesh with $40 \times 160 = 6400$ linear finite elements and

the modified integration rule (or the averaged mass matrix), the size of the time increments at the filtering stage is $\Delta t_1 = 0.038204$ according to Eqs. (13) - (15). For a uniform mesh with $120 \times 480 = 57600$ linear finite elements and the lumped mass matrix, the size of the time increments at the filtering stage is $\Delta t_2 = 0.036717$ according to Eqs. (13) - (15). Because Δt_2 is close to Δt_1, then curves 2 and 3 (or 4) in Fig. 8 are close to each other. We should also mention that with the increase in the observation time, the effectiveness of the elements with reduced dispersion increases compared with that for the standard approach; i.e., according to Eqs. (13) - (15), for the same accuracy of numerical results, the ratio $\frac{N_{FE}^{lump}}{N_{FE}^{red}}$ is an increasing function of the observation time (N_{FE}^{lump} and N_{FE}^{red} are the numbers of finite elements used with the standard formulation and with the formulations with reduced dispersion).

4 CONCLUSIONS

- The numerical techniques with reduced dispersion based on explicit time-integration methods significantly reduce the number of degrees of freedom compared with the standard finite elements at the same accuracy (e.g., by a factor of 3 in the 1-D case and 9 in the 2-D case and 27 in the 3-D case. This leads to a huge reduction in the computation time;

- The two-stage time-integration technique recently suggested in our papers [19, 20, 22] yields accurate numerical results for elastodynamics problems solved with different space-discretization approaches such as the linear elements with reduced dispersion, the spectral low- and high-order elements, the isogeometric elements;

- Except the known case of of the linear elements with the lumped mass matrix, all other space-discretization techniques considered in the paper require small time-increments for time integration at the stage of basic computations;

- The comparison of the space-discretization techniques based on the diagonal mass matrices (used with explicit time-integration methods) show that at the same number of dof, the spectral high-oder elements yield more accurate results compared with the standard linear and quadratic finite elements and the linear elements with reduced dispersion. However, when we compare the computational costs at the same accuracy, the numerical results show the the linear elements with reduced dispersion are more computationally effective than the spectral high-order elements. We should also mention that compared with the spectral 10th-order elements,the computational effectiveness of the linear elements with reduced dispersion decreases with the increase in the observation time;

- It is interesting to note that the size of time increments at the filtering stage of the two-stage time-integration technique (this size is calculated according to Eqs. (13) - (15) from the Appendix) defines the range of actual frequencies used in numerical solutions and can serve as a quantitative measure for the comparison and prediction of the accuracy and the computational effectiveness of different space-discretization techniques.

ACKNOWLEDGMENTS

The research has been supported in part by the Air Force Office of Scientific Research (contract FA9550-12-1-0324) and by Texas Tech University. The technical assistance of P. Duc is appreciated.

APPENDIX. THE TWO-STAGE TIME-INTEGRATION TECHNIQUE WITH FILTERING SPURIOUS OSCILLATIONS (see [19, 22, 20])

In order to filter spurious high-frequency oscillations, numerical dissipation (or artificial damping) is usually introduced for the time integration of Eq. (1). As we showed in our paper [20], the use of a time-integration method with numerical dissipation (or artificial damping) at each time increment leads to inaccurate numerical results for low frequencies as well, especially for a long-term integration. It is also unclear in this case how to select the amount numerical dissipation and the range of high frequencies to be filtered.

To resolve these issues, we have developed the two-stage time-integration technique (see [19, 22, 20]) with the stage of basic computations and the filtering stage. This technique is based on the fact that for linear elastodynamics problems, there is no necessity to filter spurious oscillations at each time increment because the errors in high frequencies do not affect the accuracy of low frequencies during time integration; see [20]. In the current paper, we use the standard explicit central-difference time-integration method (without numerical dissipation or artificial viscosity) at basic computations in order to obtain an accurate solution of the semi-discrete elastodynamics problem, Eq. (1) (this solution contains spurious high-frequency oscillations). We should mention that other known explicit time-integration methods can be also used for basic computations (however, in this case the dispersion analysis should be modified for the corresponding explicit time-integration method). For the filtering of spurious oscillations, the implicit TCG method with large numerical dissipation developed in [20] is used at the filtering stage. For all elastodynamics problem, we use $N = 10$ uniform time increments (5 positive plus 5 negative time increments) at the filtering stage. This means that there is no real time integration at the filtering stage (the sum of 10 time increments used at the filtering stage is zero). As shown in [20], this procedure is equivalent to the multiplication of each velocity and displacement of the uncoupled system of the semi-discrete equations by a factor of $\left(\frac{(3+m)^2+\Omega^2}{(3+m)^2+(2+m)^2\Omega^2}\right)^5$ (where $\Omega = \omega_j \Delta t$ and ω_j are the eigen-frequencies of the semi-discrete system, Δt is the time increment as well as $m = 15$ is used) and does not require the modal decomposition and the calculation of eigen-frequencies. As can be seen, this factor is close to zero for large Ω and is close to unity for small Ω. The size Δt of time increments at the filtering stage indirectly defines the amount of numerical dissipation and the range of spurious oscillations and is calculated according to the following formulas (for uniform meshes)

$$\Delta t = \alpha(\frac{c_o T}{dx}) \frac{dx \Omega_{0.1}(N)}{c_o}\,, \tag{13}$$

with

$$\alpha(\frac{c_o T}{dx}) = a_1 \left(\frac{c_o T}{dx}\right)^{a_2} \tag{14}$$

in the 1-D case and

$$\Delta t = \max_{m,j} \left[\alpha(\frac{c_m T}{dx_j}) \frac{dx_j}{c_m}\right] \Omega_{0.1}(N) = \max_{m,j} \left[\frac{dx_j}{c_m}\right]^{1-a_2} a_1\, T^{a_2}\, \Omega_{0.1}(N)$$
$$= \left[\frac{\max\limits_j dx_j}{\min\limits_m c_m}\right]^{1-a_2} a_1\, T^{a_2}\, \Omega_{0.1}(N) = \left[\frac{dx_{max}}{c_2}\right]^{1-a_2} a_1\, T^{a_2}\, \Omega_{0.1}(N)\,, \tag{15}$$

in the 2-D and 3-D cases (see our papers [22, 20]). Here, $c_o = \sqrt{\frac{E}{\rho}}$ is the wave velocity; dx is the size of a finite element in the 1-D case; T is the observation time; $c_2 = \min\limits_m c_m$ $(i = 1, 2)$

is the minimum value between the velocities of the compressional wave c_1 and the shear wave c_2; $dx_{max} = \max\limits_j dx_j$ is the maximum dimension of finite elements along the axes x_j ($j = 1, 2$ for 2-D problems and $j = 1, 2, 3$ for 3-D problems); $\Omega_{0.1}(N = 10) = 0.81$ for the TCG method with $N = 10$ time increments. Eq. (15) is based on Eqs. (13) and (14) with the selection of the maximum size of a time increment with respect to the compressional and shear waves, and the maximum size of a finite element along the coordinate axes. Using the calibration procedure described in [22], we found the following coefficients a_1 and a_2 for linear elements with the averaged ($\gamma = \frac{3-\tau^2}{2}$) mass matrix or the modified integration rule: $a_1 = 0.3296$ and $a_2 = 0.218$ for the explicit time-integration method as in the current paper and $a_1 = 0.2942$ and $a_2 = 0.2104$ for the implicit time-integration method as in our paper [17]; for the standard explicit time integration with linear elements and the lumped mass matrix: $a_1 = 0.3342$ and $a_2 = 0.3363$ (see our paper [16]). The coefficients a_1 and a_2 for the spectral and isogeometric elements are presented in our paper [15]. These coefficients a_1 and a_2 are calibrated in the 1-D case for the filtering of numerical results obtained at basic computations with very small time increments. In order to use the same coefficients a_1 and a_2 in the 2-D and 3-D cases, small time increments should be used at basic computations for the 2-D and 3-D problems. We should also mention that the filtering stage can be applied in the beginning of calculations as a pre-processor, in the end of calculations as a post-processor or at some intermediate time (see [17, 18, 20, 16] for numerous examples of the application of the two-stage time-integration technique).

REFERENCES

[1] I. Babuska, F. Ihlenburg, T. Strouboulis, and S. K. Gangaraj. Posteriori error estimation for finite element solutions of helmholtz' equation - part ii: estimation of the pollution error. *International Journal for Numerical Methods in Engineering*, 40(21):3883–3900, 1997.

[2] I. Babuska, T. Strouboulis, S. K. Gangaraj, and C. S. Upadhyay. Pollution error in the h-version of the finite element method and the local quality of the recovered derivatives. *Computer Methods in Applied Mechanics and Engineering*, 140(1-2):1–37, 1997.

[3] K. J. Bathe. *Finite element procedures*. Prentice-Hall Inc., Upper Saddle River, New Jersey, 1996.

[4] D. J. Benson, Y. Bazilevs, E. De Luycker, M.-C. Hsu, M. Scott, T. J. R. Hughes, and T. Belytschko. A generalized finite element formulation for arbitrary basis functions: From isogeometric analysis to xfem. *International Journal for Numerical Methods in Engineering*, 83(6):765–785, 2010.

[5] D.J. Benson, Y. Bazilevs, M.-C. Hsu, and T.J.R. Hughes. A large deformation, rotation-free, isogeometric shell. *Computer Methods in Applied Mechanics and Engineering*, 200(1316):1367 – 1378, 2011.

[6] F. Casadei, E. Gabellini, G. Fotia, F. Maggio, and A. Quarteroni. A mortar spectral/finite element method for complex 2d and 3d elastodynamic problems. *Computer Methods in Applied Mechanics and Engineering*, 191(45):5119–5148, 2002.

[7] H. P. Cherukuri. Dispersion analysis of numerical approximations to plane wave motions in an isotropic elastic solid. *Computational Mechanics*, 25(4):317–328, 2000.

[8] J.A. Cottrell, A. Reali, Y. Bazilevs, and T.J.R. Hughes. Isogeometric analysis of structural vibrations. *Computer Methods in Applied Mechanics and Engineering*, 195(41-43):5257 – 5296, 2006.

[9] W. Dauksher and A. F. Emery. Solution of elastostatic and elastodynamic problems with chebyshev spectral finite elements. *Computer Methods in Applied Mechanics and Engineering*, 188(1):217–233, 2000.

[10] A. Deraemaeker, I. Babuska, and P. Bouillard. Dispersion and pollution of the fem solution for the helmholtz equation in one, two and three dimensions. *International Journal for Numerical Methods in Engineering*, 46(4):471–499, 1999.

[11] D. Gabriel, J. Plesek, R. Kolman, , and F. Vales. Dispersion of elastic waves in the contactimpact problem of a long cylinder. *Journal of Computational and Applied Mathematics*, 234:1930–1936, 2010.

[12] Z. C. He, A. G. Cheng, G. Y. Zhang, Z. H. Zhong, and G. R. Liu. Dispersion error reduction for acoustic problems using the edge-based smoothed finite element method (esfem). *International Journal for Numerical Methods in Engineering*, 86(11):1322–1338, 2011.

[13] T. J. R Hughes. *The Finite Element Method: Linear Static and Dynamic Finite Element Analysis*. Prentice- Hall, Englewood Cliffs, NJ,, 1987.

[14] T.J.R. Hughes, A. Reali, and G. Sangalli. Duality and unified analysis of discrete approximations in structural dynamics and wave propagation: Comparison of p-method finite elements with k-method nurbs. *Computer Methods in Applied Mechanics and Engineering*, 197(49-50):4104 – 4124, 2008.

[15] A. Idesman, P. Duc, J. R. Foley, and M. Schmidt. The comparative study of different orders of the standard, spectral and isogeometric finite elements as well as the linear elements with reduced dispersion used for the solution of elastodynamics problems. *Computational Mechanics*, 2013 (submitted).

[16] A. Idesman, M. Schmidt, and J. R. Foley. Accurate 3-d finite element simulation of elastic wave propagation with the combination of explicit and implicit time-integration methods. *Wave Motion*, 48:625–633, 2011.

[17] A. Idesman, M. Schmidt, and J. R. Foley. Accurate finite element modeling of linear elastodynamics problems with the reduced dispersion error. *Computational Mechanics*, 47:555–572, 2011.

[18] A. Idesman, K. Subramanian, M. Schmidt, J. R. Foley, Y. Tu, and R. L. Sierakowski. Finite element simulation of wave propagation in an axisymmetric bar. *Journal of Sound and Vibration*, 329:2851–2872, 2010.

[19] A. V. Idesman. A new high-order accurate continuous galerkin method for linear elastodynamics problems. *Computational Mechanics*, 40:261–279, 2007.

[20] A. V. Idesman. Accurate time integration of linear elastodynamics problems. *Computer Modeling in Engineering & Sciences*, 71(2):111–148, 2011.

[21] A. V. Idesman and D. Pham. Finite element modeling of linear elastodynamics problems with explicit time-integration methods and linear elements with the reduced dispersion error. *Computer Methods in Applied Mechanics and Engineering*, pages 1–33, 2013 (submitted).

[22] A. V. Idesman, H. Samajder, E. Aulisa, and P. Seshaiyer. Benchmark problems for wave propagation in elastic materials. *Computational Mechanics*, 43(6):797–814, 2009.

[23] D. Komatitsch, C. Barnes, and J. Tromp. Simulation of anisotropic wave propagation based upon a spectral element method. *Geophysics*, 65(4):1251–1260, 2000.

[24] Dimitri Komatitsch and Jean-Pierre Vilotte. Spectral element method: an efficient tool to simulate the seismic response of 2d and 3d geological structures. *Bulletin of the Seismological Society of America*, 88(2):368 – 392, 1998.

[25] Dimitri Komatitsch, Jean-Pierre Vilotte, Rossana Vai, JOSE M. Castillo-Covarrubias, and Francisco J. Sanchez-Sesma. The spectral element method for elastic wave equations - application to 2-d and 3-d seismic problems. *International Journal for Numerical Methods in Engineering*, 45(9):1139 – 1164, 1999.

[26] S. Krenk. Dispersion-corrected explicit integration of the wave equation. *Computer Methods in Applied Mechanics and Engineering*, 191:975–987, 2001.

[27] K. J. Marfurt. Accuracy of finite difference and finite element modeling of the scalar and elastic wave equation. *Geophysics*, 49:533–549, 1984.

[28] R. Mullen and T. Belytschko. Dispersion analysis of finite element semidiscretizations of the two-dimensional wave equation. *International Journal for Numerical Methods in Engineering*, 18:11–29, 1982.

[29] C. Pozrikidis. *Introduction to Finite and Spectral Element Methods Using MATLAB*. CRC Press, 2005.

[30] G. Seriani and S. P. Oliveira. Optimal blended spectral-element operators for acoustic wave modeling. *Geophysics*, 72(5):95–106, 2007.

[31] G. Seriani and S. P. Oliveira. Dispersion analysis of spectral element methods for elastic wave propagation. *Wave Motion*, 45(6):729–744, 2008.

[32] B. Yue and M. N. Guddati. Dispersion-reducing finite elements for transient acoustics. *Journal of the Acoustical Society of America*, 118(4):2132–2141, 2005.

[33] O. C. Zienkiewicz and R. L. Taylor. *The Finite Element Method*. Butterworth-Heinemann, Oxford, UK, 2000.